separations

MDPI

Article

Polyaniline/Glauconite Nanocomposite Adsorbent for Congo Red Dye from Textile Wastewater

Doaa Salah [1], Ahmed Hamd [2,*], N. K. Soliman [2], Ali M. Elzanaty [1], Abdulaziz M. Alanazi [3], Mohamed Shaban [4,*], Refat El-Sayed [5,6] and Sayed A. Ahmed [1,7]

1 Department of Chemistry, Faculty of Science, Beni-Suef University, Beni-Suef 62511, Egypt
2 Basic Science Department, Faculty of Oral and Dental Medicine, Nada University, Beni-Suef 62764, Egypt
3 Department of Chemistry, Faculty of Science, Islamic University of Madinah, Madinah 42351, Saudi Arabia
4 Department of Physics, Faculty of Science, Islamic University of Madinah, Madinah 42351, Saudi Arabia
5 Department of Chemistry, University College in Al-Jamoum, Umm Al-Qura University, Makkah 25376, Saudi Arabia
6 Chemistry Department, Faculty of Science, Benha University, Benha 13518, Egypt
7 Basic Science Department, Faculty of Engineering, Nahda University, Beni-Suef 62764, Egypt
* Correspondence: ahmed.hamd@nub.edu.eg (A.H.); mssfadel@aucegypt.edu (M.S.)

Abstract: Glauconite (Gl), a naturally occurring clay material, was utilized as an affordable and ecologically friendly adsorbent to explore its capturing capacity towards Congo red (CR) dye from textile industrial waste effluent. To improve adsorption and removal effectiveness, a modification technique utilizing polyaniline (PAN) was investigated. An X-ray diffractometer (XRD), a scanning electron microscope (SEM), and Fourier transformer infrared (FTI-R) were applied as strong familiar characterization techniques for all used adsorbents. The effects of starting concentration, contact duration, adsorbent dose, pH, and temperature on the adsorption process were also studied. The reusability of the adsorbent was studied over four adsorption cycles. The results show that PAN modification of Gl enhances the effectiveness of CR elimination. The clearance efficiency of raw and modified glauconite at 25 °C and pH 7 was 77% and 91%, respectively. The kinetics and isotherms of Congo red dye adsorption were investigated using batch studies to determine the impacts of various experimental conditions. The maximum adsorption capacity of the glauconite/polyaniline (Gl/PAN) nanocomposite rose from 11.9 mg/g for Gl to 14.1 mg/g in accordance with the isotherm analysis, which shows that the Langmuir isotherm properly characterizes the experimental data. The pseudo-second-order model (R^2 = 0.998) properly expresses the experimental data. The reusability research proved that the adsorbents may be reused effectively. The overall results suggest that the modified Gl by PAN might be used as a low-cost, natural adsorbent for eliminating CR color from textile effluent.

Keywords: polyaniline; glauconite; nanocomposites; adsorbents; water treatment; Congo red dye

Citation: Salah, D.; Hamd, A.; Soliman, N.K.; Elzanaty, A.M.; Alanazi, A.M.; Shaban, M.; El-Sayed, R.; Ahmed, S.A. Polyaniline/Glauconite Nanocomposite Adsorbent for Congo Red Dye from Textile Wastewater. *Separations* **2022**, *9*, 384. https://doi.org/10.3390/separations9110384

Academic Editor: Xinhua Qi

Received: 4 October 2022
Accepted: 10 November 2022
Published: 21 November 2022

1. Introduction

The issue of chemical pollution in water has become more significant to society, the government, and—more importantly—the whole industrial world [1–5]. Numerous factors contribute to water pollution, including energy consumption, radioactive waste, urban growth, pesticides and chemical fertilizers, industrial waste, mining operations, sewage, and wastewater [4,6–9]. Dye is one of these contaminants. Synthetic dyes are widely utilized in a variety of high-tech sectors, including those that produce plastics, cosmetics, rubber, paper and other types of textiles, as well as leather tanning and food processing, and printing [10–15]. Thus, treating effluents has become essential for the industrial sector. Familiar physical, chemical, and biological technologies including biodegradation, phytoremediation, membrane filtration, electrochemistry, evaporation, carbon adsorption, ion exchange, oxidation, solvent extraction, flotation, and

precipitation methods have been extensively used as efficient methods for removing these pollutants over the past three decades [4,5,7,16–23]. Due to its environmental and financial sustainability, dye removal by adsorption is the most efficient and functionally practicable of all these methods [8,24,25]. Numerous widely accessible and abundant naturally occurring substances have been investigated as adsorbents for the removal of dyes from wastewater [26–28]. For the treatment of wastewater polluted with dye, there is rising interest in the use of inexpensive, easily accessible clays and clay-modified adsorbents, including diverse natural materials and waste products from industry or agriculture [29–31]. In the last 10 years, the advancement of nanotechnology has demonstrated incredible promise for use in solving environmental issues. Owing to their individual and unique physical and chemical properties—more precisely their noticeable elevated ratio between specific surface area and volume, high capacity, high selectivity, and a large number of active groups that can be used for binding heavy metals—nanomaterials have been extensively used as high-efficiency adsorbents for removing dyes and heavy metals [32]. These nanomaterials, however, have run into several problems, including high cost, nano-toxicity, poor separation and recovery efficiency after usage, etc. They may also produce new contaminants that have a detrimental effect on ecosystems and living things [33]. Incorporating nanoparticles into a different matrix to create a heterogeneous solid nanocomposite is an efficient technique to get around some of these restrictions [34]. Due to its widespread availability, low cost, and minimal impact on the environment, nano clay has been explored in a variety of academic fields. A layered structure of nanoparticles called nanoclay is made up of octahedral aluminum flakes and one or two tetrahedral silicon dioxide flakes. Functional molecules can be anchored to the clay surface. However, they have relatively little ability to adsorb heavy metals from aqueous solutions. Polyaniline polymers are mixed with raw clay or other composites to create nanocomposites that combine the unique properties of each matrix and enhance their adsorption capacity and structural characteristics [35–37].

Glauconite is a phyllosilicate heterogeneous mineral sediment with a documented chemical formula of $(K,Na)(Fe,Al,Mg)_2(Si,Al)_4O_{10}(OH)_2$. Due to its bluish-green to greenish-black color, glauconite has several names like green clay, green sand, or green earth [38]. The chemical analysis of glauconite indicated that the main components were SiO_2 (50.52%), Fe_2O_3 (20.17%), K_2O (8.40%), Al_2O_3 (6.04%), and Mg_O (4.2%) [39]. The popularity of glauconite clay as an adsorbent in water treatment applications for the removal of various metal ions and dyes has been documented by several researchers [40,41]. In this research, environmentally friendly and low-cost raw materials (Gl, PAN, and HCl) were used to prepare the Gl/PAN nanocomposite. To determine the optimum adsorbent technology for efficiently removing and retaining waste dyes, particularly CR dye, from industrial wastewater, this nanocomposite will be used in wastewater treatment with an emphasis on CR dye. Adsorption kinetics, effects of several factors including CR dye removal, and isotherms were examined in batch mode testing. These factors included starting CR dye concentration, contact duration, adsorbent doses, pH changes, and temperature gradient.

2. Materials and Methods

2.1. Raw Materials, Dyes, and Reagents

Glauconite was donated by El-Nassr Company, a mining company that mines different naturally occurring ores, and uses glauconite with further modification using the polymerized form of aniline (PAN). Sodium hydroxide granules with 99% purity, hydrochloric acid (36%) which was used for pH adjustment, aniline (AN), potassium persulf (PPS), and Congo red dye were supplied with the aid of Sigma Aldritch, and all dissolving processes were applied using distilled water.

2.2. Preparation of Gl/PAN Composite

We used Gl powder with a particle size of 315 µm, polymerized on its surface using aniline that has been dissolved in HCl at a concentration of 0.1 M, and used PPS (0.1 M) as an oxidizing agent, as stated in [42,43]. The composite was created by swirling the

mixture at room temperature for two hours while taking into account the 1:1 mass ratio of Gl and PAN [43]. After a day, the mixture was filtered and carefully rinsed with distilled water to achieve a neutral pH. The resulting solid was then separated and dried in a vacuum for 24 h at 60 °C. Utilizing FTIR, XRD, and SEM, the samples of glauconite and PANI composite were analyzed. FTIR spectra were obtained using a Bruker VERTEX 70FTIR spectrophotometer using the dry KBr pellet technique. Moreover, the XRD charts were observed in the range of 10°–70° with a scan step of 0.02° utilizing a PANalytical diffractometer (Empyrean). Finally, SEM images were captured using a Quanta FEG 250 microscope (Switzerland).

2.3. Preparation of Adsorbate

Congo red (CR), our selected anionic dye, is the material to be adsorbed in this study. This dye is known as the sodium salt of 3, 30-([1, 10-biphenyl]-4, 40-diyl) bis (4-amino naphthalene-1-sulfonic acid) with a formula: $C_{32}H_{22}N_6Na_2O_6S_2$ as shown in Figure 1. A stock solution of 1000 mg/L was prepared by dissolving the appropriate amount (1000 mg) of CR in a liter of distilled water. The working solutions were prepared by diluting the stock solution with distilled water to give the appropriate concentration of the working solutions. The pH values of the solutions were adjusted to 2, 3, 4, 6, 8, and 12 by the addition of either 0.1 M HCl or 0.1 M NaOH solutions, and measured by the pH meter.

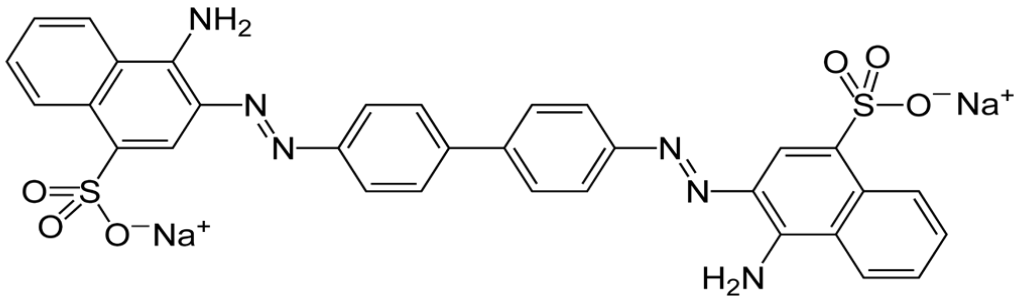

Figure 1. Structure of Congo red.

2.4. Adsorption Studies

Four series of adsorption tests were implemented on the Gl and Gl/PAN composite adsorbents using altered adsorption parameters. These parameters were: the dye initial concentration; the temperature of adsorption; dosages of adsorbents; and finally pH of the solution as shown in Table 1. All tests of CR dye adsorption were done in batch mode scale in various conditions including dye initial concentrations (5–25 mg/L), contact time (0–420 min), adsorbent dosage (0.02–0.1 g per 20 mL of CR solution), pH (2–12), and temperature (25–60 °C) for 420 min. The experiment time was set at 420 min and the volume of the solution was 20 mL in all experiments. By using a UV-Vis spectrophotometer (PerkinElmer Lambada 950), the changes in the concentration of the analyzed dye were illustrated by its characteristic absorption peaks.

Table 1. Conditions of experimental tests.

Series	Dye Concentration, ppm (mg/L)	Gl and Gl/PAN Weight, g	Temperature, °C	pH Value
1	5 10 15 20 25	0.02	25	7
2	5	0.02 0.04 0.06 0.08 0.1	25	7
3	5	0.02	25 40 50 60	7
4	5	0.02	25	2 3 4 6 7 8 12

The reusing experiments of both Gl and Gl/PAN composite adsorbents were explored 4 times using 0.02 g of all adsorbents, with 20 mL of 5 mg/L as the initial concentration

of CR for contact time 120 min 25 °C and pH 7. For each run, Gl and Gl/PAN composite adsorbents were gathered from the solution, then washed with distilled water and set for the next run.

Equations (1)–(3) were used, respectively, to calculate the amount of CR absorption uptake by the produced composite at equilibrium (q_e (mg/g)), at time t (q_t), and the amount of CR dye removal% [41,44–46]:

$$q_e = (C_o - C_e)V/m \quad (1)$$

$$q_t = (C_o - C_t)\frac{V}{m} \quad (2)$$

$$\text{CR dye removal \%} = \frac{(C_o - C_t)}{C_o} \times 100 \quad (3)$$

where C_o, C_t, and C_e stand for the initial (in mg/L), time, and equilibrium concentrations of CR, respectively. The dye volume is indicated as in milliliters, while the mass of the Gl and Gl/PAN composite is shown as in milligrams.

2.5. Adsorption Isotherm

Fitting the adsorption data with the isotherm models is critical in clarifying the adoption behavior of dissolved ions using solid adsorbents [47]. Here we investigate three isotherm models to understand the adsorption behavior of CR dye on the Gl and Gl/PAN nanocomposite. Langmuir, Freundlich, and Tempkin isotherms models were represented by Equations (4)–(6), respectively [48–53];

$$\frac{C_e}{q_e} = \frac{1}{K_L Q_o} + \frac{C_e}{Q_o} \quad (4)$$

$$\log q_e = \log K_F + \frac{1}{n}\log C_e \quad (5)$$

$$q_e = B\ \ln K_T + B\ \ln C_e \quad (6)$$

Q_o is the maximum amount of dye that Gl or Gl/PAN nanocomposite can remove. The Langmuir, Freundlich, and Tempkin binding constants are denoted by K_L, K_F, and K_T, respectively. The adsorption density is represented by **n**. The constant B is equal to RT/b, which is related to the heat of adsorption. Absolute temperature is denoted by T(K). R is the universal gas constant (8.314 J.mol^{-1} K^{-1}). Calculating the value of the dimensionless separation factor constant (R_L) from Equation (7) allows one to easily determine the degree to which the Langmuir isotherms are favorable for the equilibrium data [54],

$$R_L = \frac{1}{(1 + K_L C_{max})} \quad (7)$$

where C_{max} denotes the maximum initial CR concentration.

2.6. Adsorption Kinetics and Mechanism

The adsorption of CR onto Gl and Gl/PAN adsorbents was examined by intra-particle diffusion, pseudo-first and second order, as well as the simple Elovich kinetic model as a variety of adsorption parameters and kinetic models. Equations (8)–(11) represent the pseudo-first-order kinetics model, pseudo-second-order kinetics model, simple Elovich kinetic model, and Intra-particle diffusion model [55–60];

$$\ln (q_e - q_t) = \ln q_e - K_1\ t \quad (8)$$

$$\frac{t}{q_t} = \frac{1}{k_2 q_e^2} + \frac{t}{q_e} \quad (9)$$

$$q_t = \frac{1}{\beta} \ln \alpha\beta + \frac{1}{\beta} \ln t \quad (10)$$

$$q_t = k_3 t^{\frac{1}{2}} + I \quad (11)$$

where K_1, K_2, and K_3 represent the pseudo-first-order rate constant, pseudo-second-order rate constant, and intra-particle propagation rate constant, respectively. α refers to the adsorption rate at time = 0 min (mg/min), β represents the extent of surface coverage (g/mg), and I is a constant associated with the thickness of the boundary layer.

2.7. Statistical Analysis

The adsorption data was a mean of three independent experiments. The regression coefficient (R^2) values of Langmuir, Freundlich isotherm, pseudo-first-order, pseudo-second-order, Intra-particle diffusion, and Elovich kinetic models were determined using statistical functions of Origin Pro 2016 & Microsoft Excel, 2010 version.

3. Results and Discussion

3.1. Adsorbent Characterization

3.1.1. SEM Characterization

There are clearly discernible micro-aggregates with leaf-like patterns and crystal morphologies that had multiple mesopores [61] which enhanced the adsorption ability [39], as seen in SEM images of glauconite samples in Figure 2A,B. Figure 2B shows self assembled nanoparticles to show nanosheets of nanoporous surface as shown in the inset. The average particle size is 73 ± 4 nm. The many structural forms of typical polyaniline include flakes, granules, nanofibers, nanotubes, nanospheres, and nanofibers [62]. Figure 2C,D of Gl/PAN shows the spongy or netlike structure produced by Polyaniline chains as well as the sheets or crystals generated by the aggregation of small glauconite granules. The high amount of micropores in the composite suggests a wider liquid-solid contact, which might easily speed up the adsorption process.

3.1.2. FT-IR Analysis

Both Gl and Gl/PAN adsorbents revealed FT-IR characteristic bands which are displayed in Figure 3a. Nearly all peaks shifted or disappeared referring to the functional groups on the surface of the glauconite that were covered or interacted with the treating medium, polyaniline. The FT-IR spectrum of Gl clay revealed a broad absorption band located at 3400–3700 cm^{-1} which is attributed to the stretching and bending vibrations of –OH groups of adsorbed water molecules as well as metal hydroxides found within the structure of Gl clay [63,64]. The vibrational bands located at 802 and 1023 cm^{-1} in the adsorption spectrum refer to Fe–OH bending and Si(Al)–O–Si asymmetric stretching, respectively [65]. The bending vibration of the Si–O bond appeared at 678 cm^{-1}. Additionally, vibrational modes located at 445, 447, and 496 cm^{-1} are correlated to Si–O–Mg, Si–O–Si, and Si–O–Fe^{3+} bending vibrations, respectively [66]. Furthermore, FT-IR spectra of the Gl/PAN composite revealed two clear bands at about 1620 and 3450 cm^{-1} referring to O–H bending and stretching modes of adsorbed water molecules and metal hydroxides, indicating the formation of the hydrogen bonds in the composite [41]. Moreover, the two vibrational bands which appeared clearly at 445 and 447 cm^{-1} for the raw Gl were shifted to higher wavenumbers in the case of the prepared composites. This band shift was repeated and noticed again in case of vibrations of the silica group comprising of Si–O–Si bend and Si–O–Si symmetric and asymmetric stretches appeared at lower wavenumbers for the prepared Gl/PAN composite compared to the Gl clay [63]. These bands appeared at 447 and 496 cm^{-1} for Gl/PAN composite. The characteristic bands assigned to $–NH_2$ and –OH groups in the wavenumber range of 3409–3529 cm^{-1} were noticed in the case of the prepared Polyaniline/clay composites. The spectrum of the Gl/PAN also exhibited a vibrational band at 2948 cm^{-1}, which may be attributed to –CH stretching of polyaniline of composite that also shows the bending vibrational bands due to methylene and methyl

groups appearing in the range of 1316–1485 cm^{-1}. The vibrational band located at about 1640 cm^{-1} is probably due to the –C=O group [41]. Finally, the band located at 1421 cm^{-1} refers to the bending mode of the $–NH_2$ group.

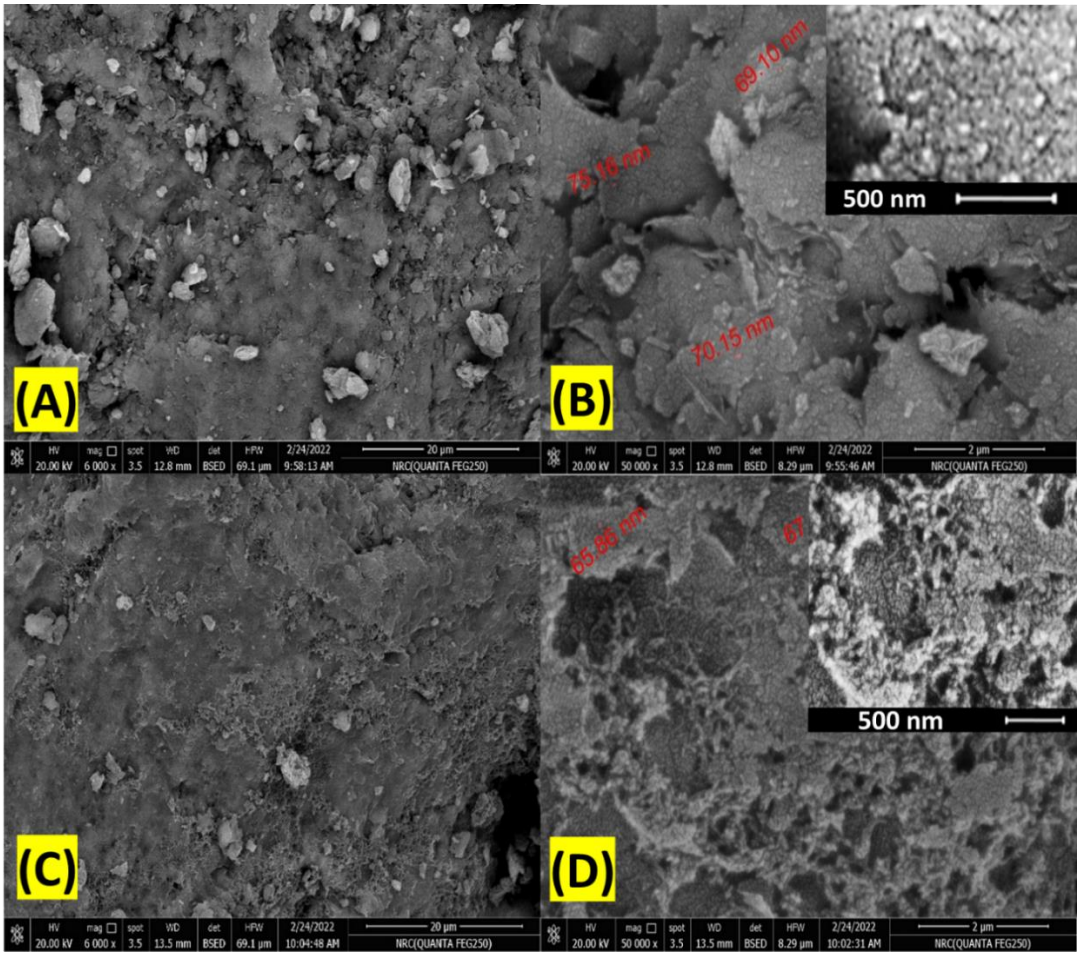

Figure 2. SEM micrograph for (**A**,**B**) Gl and (**C**,**D**) Gl/PAN nanocomposite.

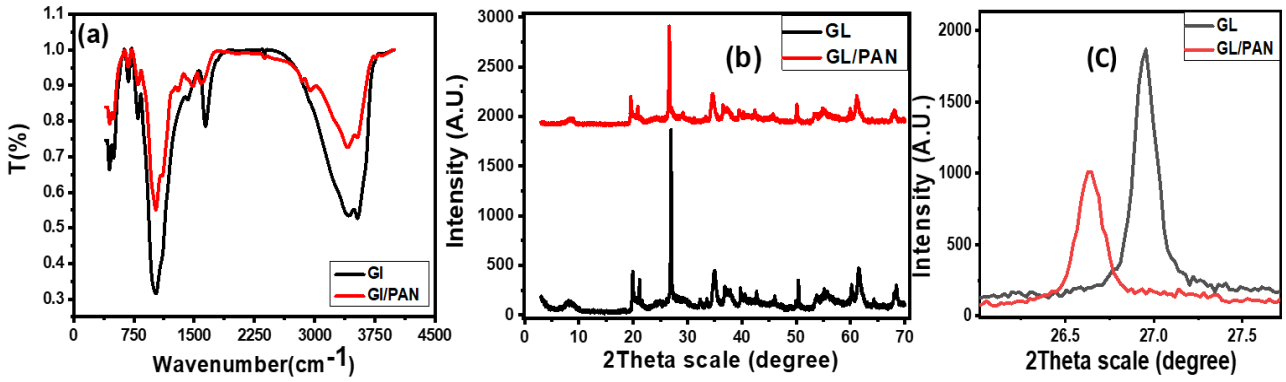

Figure 3. (**a**) F-TIR and (**b**,**c**) XRD charts of Gl and Gl/PAN adsorbents.

3.1.3. X-ray Diffraction Characterization

The X-ray Diffraction patterns for both Gl and Gl/PAN are shown in Figure 3b. Diffraction patterns for the prepared Gl/PAN composites (Figure 3b) are quite similar to that of Gl [67]. The most intense peaks at 2θ of 21.3° and 27.8° confirm the presence of Gl in the two samples. However, there is a shift of the sharp peak to 2θ = 26.6° with significant decrease in the intensity, which indicated the presence of polyaniline in the

formed composite (Figure 3c). The average crystallite sizes were calculated using the Scherer equation and were found to be 15.6 nm and 12.6 nm for Gl and Gl/PAN, in order, which refers to the presence of the nanostructures of the newly synthesized composite.

3.2. Factors Influencing the Adsorption Process

3.2.1. Effect of Initial Dye Concentration

There is a clear variation in the removal percentage and the quantity of CR dye captured by Gl and Gl/PAN adsorbents at varied initial dye concentrations and time as shown in Figure 4 which indicates that during the first stages of the adsorption process, the adsorption capacity and the removal percent were elevated till the equilibrium was reached. Thereafter, contact time has no noticeable effect on the adsorption process using new sorbents after equilibrium. The exposed active adsorption sites found on the adsorbent's surface with large quantities could be assigned for the rapid removal rate early in the reaction. The uncovered sites get fully occupied by the adsorbed CR molecules when the time of contact between adsorbent and adsorbate is increased [45].

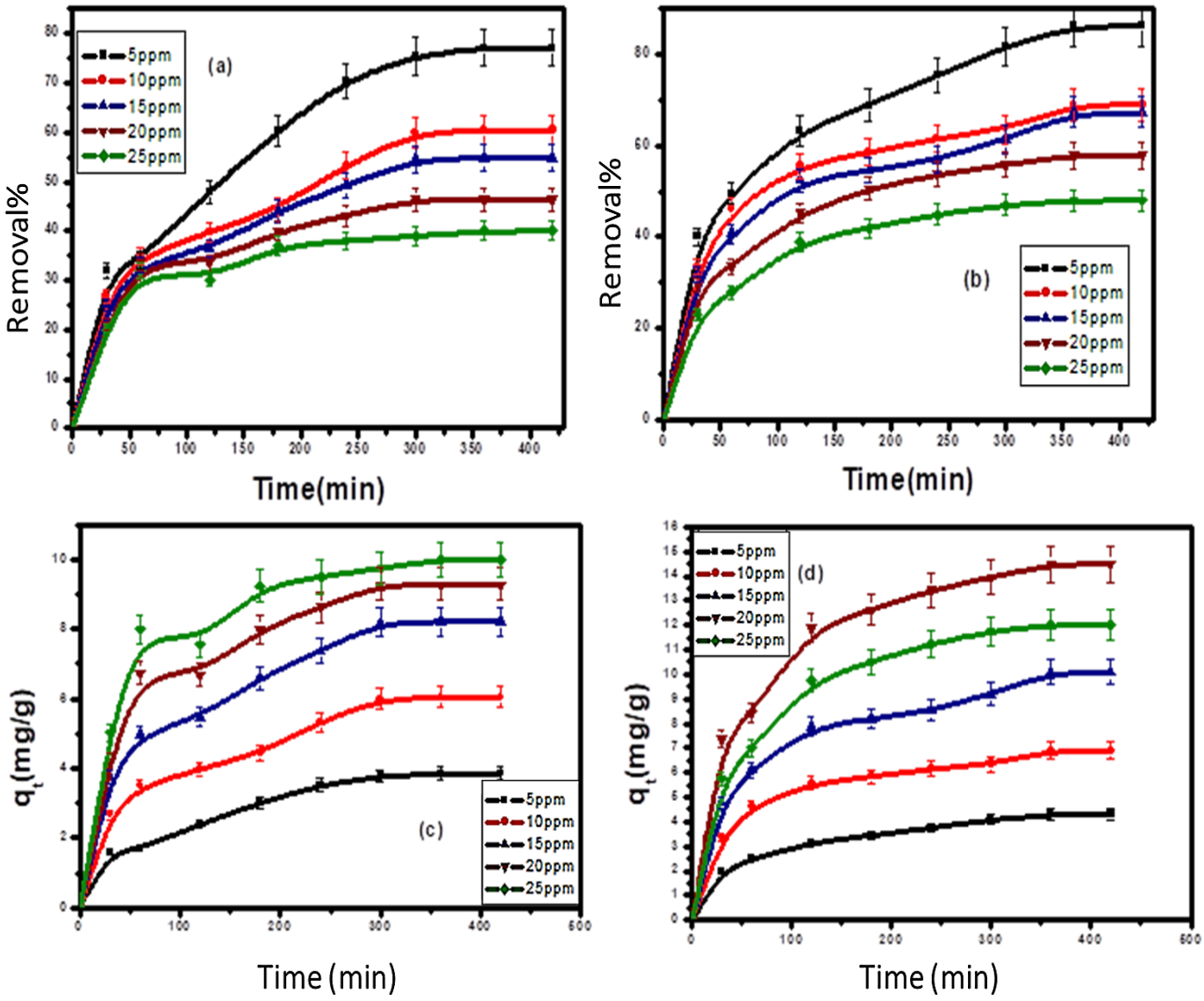

Figure 4. Effect of CR dye concentrations and contact time on the removal % and amount of adsorbed dye at 25 °C and pH 7 by 20 mg of (**a**,**c**) Gl, and (**b**,**d**) Gl/PAN nanocomposite.

The efficacy of adsorption increases with decreasing CR dye concentrations, particularly at beginning dye concentrations of 5 ppm. Glauconite had a removal percentage of 77% in Figure 4a, while Gl/PAN removal percent in Figure 4b showed maximum adsorption and removal percentage of nearly 87%. In contrast to higher concentrations, the removal percentage drops at 10, 15, 20, and 25 ppm. The elevated removal rates at an early stage of the reaction are assigned to the density of the substantial surface of uncovered active sites on the surfaces of the adsorbent. As the duration extended and the adsorbent and adsorbate were in contact with one another, the hot spots were covered step by step till become fully occupied sites by CR molecules [68,69]. Hence repulsive forces are created between CR molecules that have been adsorbed on adsorbent surfaces and the upcoming CR molecules found in the bulk liquid phase [70].

The amount of adsorbed CR increases as the initial CR concentration increases, as seen in Figure 4c,d. This might be explained by the fact that as the initial CR concentration was raised, the concentration gradient grew. As a result, the mass transfer barrier between the CR adsorbate and the Gl and Gl/PAN nanocomposite adsorbents is appropriately obscured by rising draught forces. Maximum Gl adsorption capacities were found to be 3.8, 6, 8, 2, and 10 mg/g, while Gl/PAN composite adsorption capacities were found to be 4.3, 6.8, 10, and 12 mg/g for CR with starting concentrations of 5, 10, 15, and 25 mg/L, respectively, at pH 7 and 25 °C. The outcomes demonstrated that the modification of Gl with PAN is a workable strategy to improve the effectiveness of CR elimination.

3.2.2. Effect of Adsorbent Doses

To determine the ideal adsorbent dosage that provides the greatest efficiency, the impact of adsorbent mass on CR removal percentage was evaluated to compute the adsorption cost, as illustrated graphically in Figure 5a. Adsorbent dosages varied from 0.02 to 0.1 g. It has been discovered that 0.02 g of adsorbent per 20 mL of CR solution with a starting concentration of 5 mg/l provides the maximum level of efficiency. The elimination percentage was determined to be 63.6% for Gl and 81.6% for Gl/PAN. The figure also demonstrates that the dye removal percentage in the two samples decreases with increasing the adsorbent dose from 0.02 to 0.1 g, with the removal percentage in the Gl/PAN composite decreasing to 69.2% with an increase in dose to 0.04 g and continuing to decrease to 40.8% with a high dose of 0.1 gm. As the adsorbent dose increased to 0.04 gm, the removal percentage dropped to 45.2%, and it continued to fall until it reached 32% with 0.1 g of Gl adsorbent. The screen effect, which happens when the adsorbent dose is raised and a dense layer builds on the adsorbent surface owing to the accumulation of adsorbent particles and the reduction in the space between adsorbent molecules, may help to explain this behavior. A condensed coating on the surface of the adsorbent prevented CR molecules from reaching the binding sites. The few binding sites for CR molecules were also a source of competition due to the overlap between Gl and Gl/PAN. Agglomeration or aggregation at higher adsorbent dosages lengthens the diffusion channel for CR adsorption, which reduces the adsorption percentage [71–74].

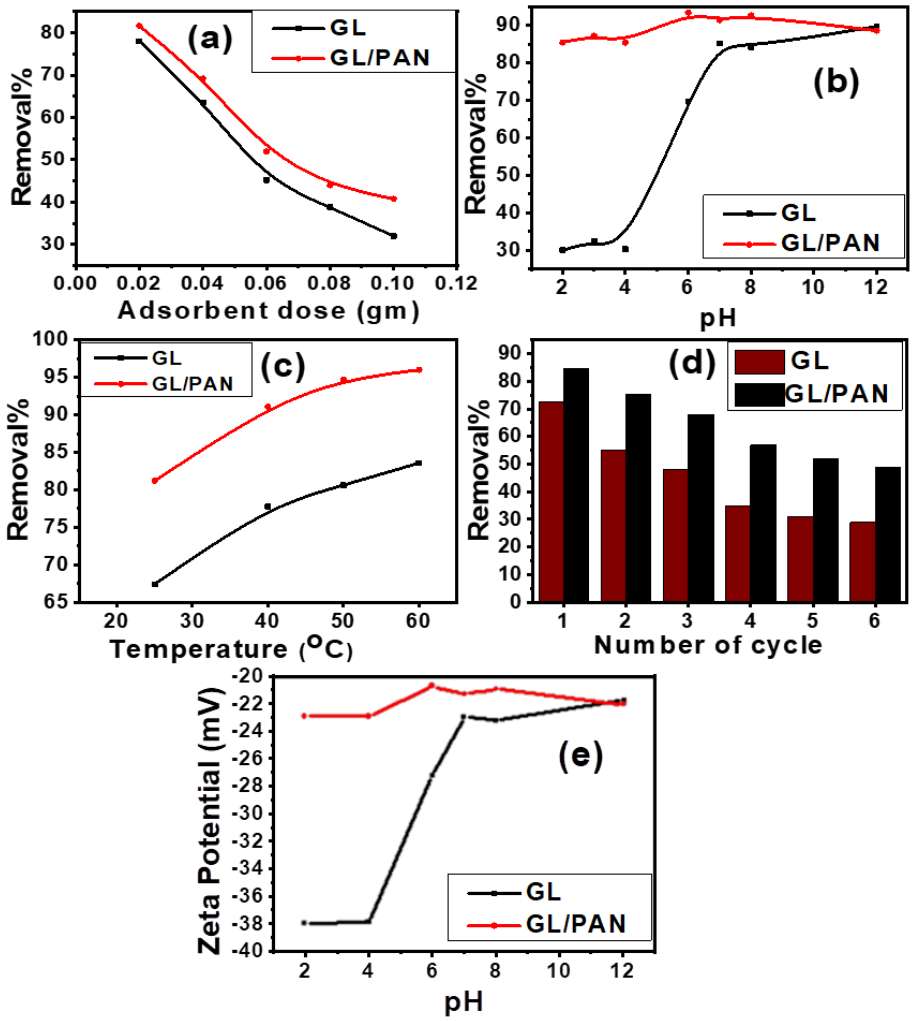

Figure 5. Effect of adsorption conditions on the removal% of CR dye (20 mL and 5 mg/L) by Gl and Gl/PAN composite: (**a**) effect of adsorbent weight; (**b**) effect of initial pH of the solution; (**c**) effect of adsorption temperature; (**d**) effect of the reusability test; and (**e**) zeta potential measurements as a function of pH for GL and GL/PAN.

3.2.3. Effect of Solution pH

The efficacy of adsorption is reliant on the solution pH because the difference in pH leads to variations in the degree of ionization of the adsorptive molecule and the adsorbent's surface characteristics [75]. A pH range from 2 to 12 was selected to study the effect of pH on the CR removal efficiency of the adsorbent as shown in Figure 5b. Gl adsorbent shows removal percentages of 30%, 32.4%, 69.6%, 85.0%, and 89.0% for investigated dye with initial concentration 5 mg/L, sorbent dosage 0.02 g of Gl per 20 mL of CR solution at pH values of 2, 3, 6, 7, and 12, in that order. Meanwhile the Gl/PAN adsorbent shows removal percentages of 85.5%, 87.0%, 93.4%, 91.4%, and 88.6% under the same previously mentioned conditions. In the case of Gl/PAN, the CR removal % increases as the pH of the CR solution increased to reach the highest value at pH 7. The lower removal % in acidic media may be attributed to the presence of high mobility of H^+ ions and the adsorbent surface protonation. As a result of competition between H+ ions and CR molecules during the adsorption process, the percentage of CR elimination drops [76]. The approximately steady removal percent at high pH values is in agreement with the previously published results [77,78] and also agrees well with the suggestion that if the maximum limit of dye removal was attained by the adsorbent, there will be no effect achieved by increasing the adsorbent dose [79]. For Gl, the highest removal % at pH 12 decreases due to the value of

H^+ ions concentration; hence, an elevation in the CR removal % by all adsorbents takes place [80]. To find out the effect of pH on Gl and Gl/PAN, their zeta potentials in solution were studied. Figure 5e shows the effect of pH on the zeta potential of Gl and Gl/PAN in an aqueous solution. Figure 4e reveals that Gl and Gl/PAN acquired negative surface charges in the pH range of 2–12. The more the pH range increased from 2 to 12, the higher the surface charge value of the GI, which resulted in a gradual increase in the electrostatic attraction between the adsorbent and the negatively charged CR. Large fluctuations in adsorption capacity were observed in the pH range of 4 to 7 indicating large changes in zeta potential. Generally, a higher zeta potential value moves towards a positive value, reflecting a greater removal %. The lower zeta potential indicates that the adsorbent surface is partially negatively charged at pH 2 to 10, and the electrostatic forces between Gl and Gl/PAN and CR through the sulfonic acid groups (SO^{3-}) are mainly repulsive during the experiment [20]. In other words, as the pH of the system increases, the number of negatively charged sites on the adsorbent surface decreases, while the number of positively charged sites on the adsorbent surface increases. Therefore at higher pH the positively charged surface has a rather high electrostatic interaction with the anionic dye, which increases adsorption. In the pH range studied, in the case of both Gl and Gl/PAN, no pH values at which the sorbent has zero point charge (pHzpc) were detected.

3.2.4. Effect of Temperature

The effect of temperature on CR dye adsorption is regarded as an additional considerable physicochemical factor since it usually causes variation in the adsorption capability of the adsorbent [81]. The effect of temperature on the capturing capability of Gl and Gl/PAN to CR dye was evaluated at different adsorption temperatures. These temperatures were selected to be 25, 40, 50, and 60 °C, and the results are revealed clearly in Figure 5c. The CR removal % by Gl is increased from 76.4% to 83.4% with increasing the temperature from 25 to 60 °C. But, in the case of Gl/PAN nanocomposite, the removal % increased from 81.2% to 96% with increasing the temperature from 25 to 60 °C. This performance may be owed to the growth in the CR diffusion rate with increasing the applied temperature as a result of the decrease in the viscosity of the solution [82]. As a result, it is found that the CR dye adsorption increases as the temperature rises, indicating that CR removal is greater at relatively high temperatures. More molecules may gather sufficient energy to interact with active regions on the composite surface. Additionally, the composite's interior structure may enlarge as a result of the elevated temperature, making it easier for dye molecules to flow through [83].

3.2.5. Reusability of Adsorbents

Four repeated experiments were done to investigate the reusability of the GI and Gl/PAN adsorbents for the capturing of CR dye with the same adsorbent and the same adsorbent dosage, Figure 5d. The findings demonstrated that, during the four adsorption cycles, the removal strength of every utilized adsorbent significantly fluctuated. The documented dye removal percentages for Gl adsorbent were 72.5, 55, 48%, 35%, 31%, and 29% from the first to the sixth cycle, respectively. The dye removal percentage for Gl/PAN adsorbent falls from 85% and 75.5% for cycles 1 and 2 to 68% and 57% for cycles 3 and 4, and from 52% to 49% for cycles 5 and 6, respectively. The CR removal percentage may decrease due to the clusters created by the assistance of CR molecules on the adsorbent surface, which provide a shield on the Gl and Gl/PAN adsorbent surface and pores, and provide protection from the dissolved CR molecules [84].

3.3. Adsorption Isotherm

The data fitting to Langmuir, Freundlich, and Tempkin isotherms was assessed using the statistical significance of R^2 (correlation coefficient) for linear plots of Ce/qe versus Ce, log qe against log Ce, and qe against Ln Ce, respectively. The computed values of Qo, K_L, K_F, 1/n, K_T, B, and R^2 were derived from the linear plots in Figure 6 and reported in Table 2.

The data show that the Langmuir isotherm models with the highest R^2 values are followed by CR adsorption on Gl and Gl/PAN composite adsorbents. As a result, the adsorbed CR molecules do not interact with one another and the dye is eliminated at the active sites of the Gl and Gl/PAN adsorbents on a single surface layer. The R^2 values for the Gl and Gl/PAN Langmuir isotherms at 25 °C are 0.9908, 0.9822, and 0.9822, respectively. Since R_L is less than 1, it may be concluded that CR adsorption is advantageous in the scenario under study [85]. The Langmuir isotherm model predicted that the highest amounts of CR adsorbed on the surfaces of Gl and Gl/PAN would be 11.90 and 14.09 mg/g respectively. The values of (1/n) in the Freundlich isotherm model for CR adsorption on adsorbents are smaller than unity in the adsorption process.

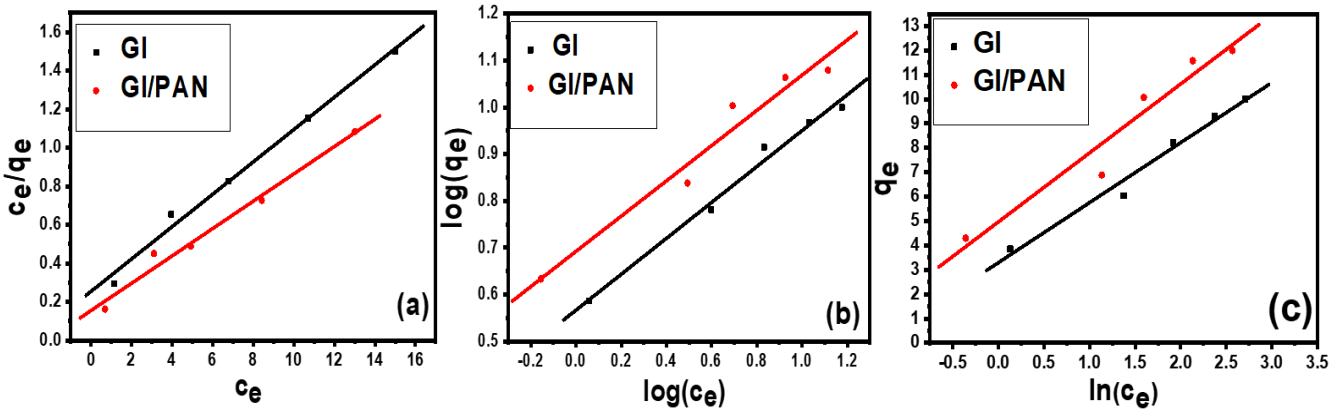

Figure 6. Plots of adsorption isotherms for the adsorption of CR dye by 50 mg of Gl, and Gl/PAN composite at 25 °C and initial pH 7: (**a**) Langmuir isotherms model; (**b**) Freundlich isotherms model; and (**c**) Tempkin isotherms model.

Table 2. Isotherm parameters for CR adsorption on Gl and Gl/PAN.

Langmuir isotherm					
Adsorbent \ Constant	Q_o (mg/g)	K_L (L/mg)	**Sd(yE±)**	R_L	R^2
Gl	11.90	0.3300	0.46235	0.9954	0.9908
Gl/PAN	14.09	0.4582	0.34417	0.9910	0.9822
Freundlich isotherm					
Adsorbent \ constant	n	K_f	**Sd(yE±)**	R^2	
Gl	2.60	3.6886	0.16929	0.9877	
Gl/PAN	2.65	4.9243	0.18817	0.9598	
Tempkin isotherm					
Adsorbent \ constant	B(J/mole)	KT(L/mole)	**Sd(yE±)**	R^2	
Gl	2.4644	3.8018	2.51557	0.9790	
Gl/PAN	2.8336	5.7621	3.29188	0.9417	

3.4. Adsorption Kinetics

The adsorption process of CR on Gl and Gl/PAN was studied under various initial dye concentrations to determine the most appropriate adsorption kinetics model. Figure 7 shows the first-order, second-order, and Elovich kinetics linear graphs, respectively, by plotting ln ($q_e - q_t$) versus t, t/q_t versus t, and q_t versus ln(t), respectively. Table 3 shows the adsorption kinetics parameters (k_1, k_2, q_e, β, and α) of the assessment models, as well as R^2.

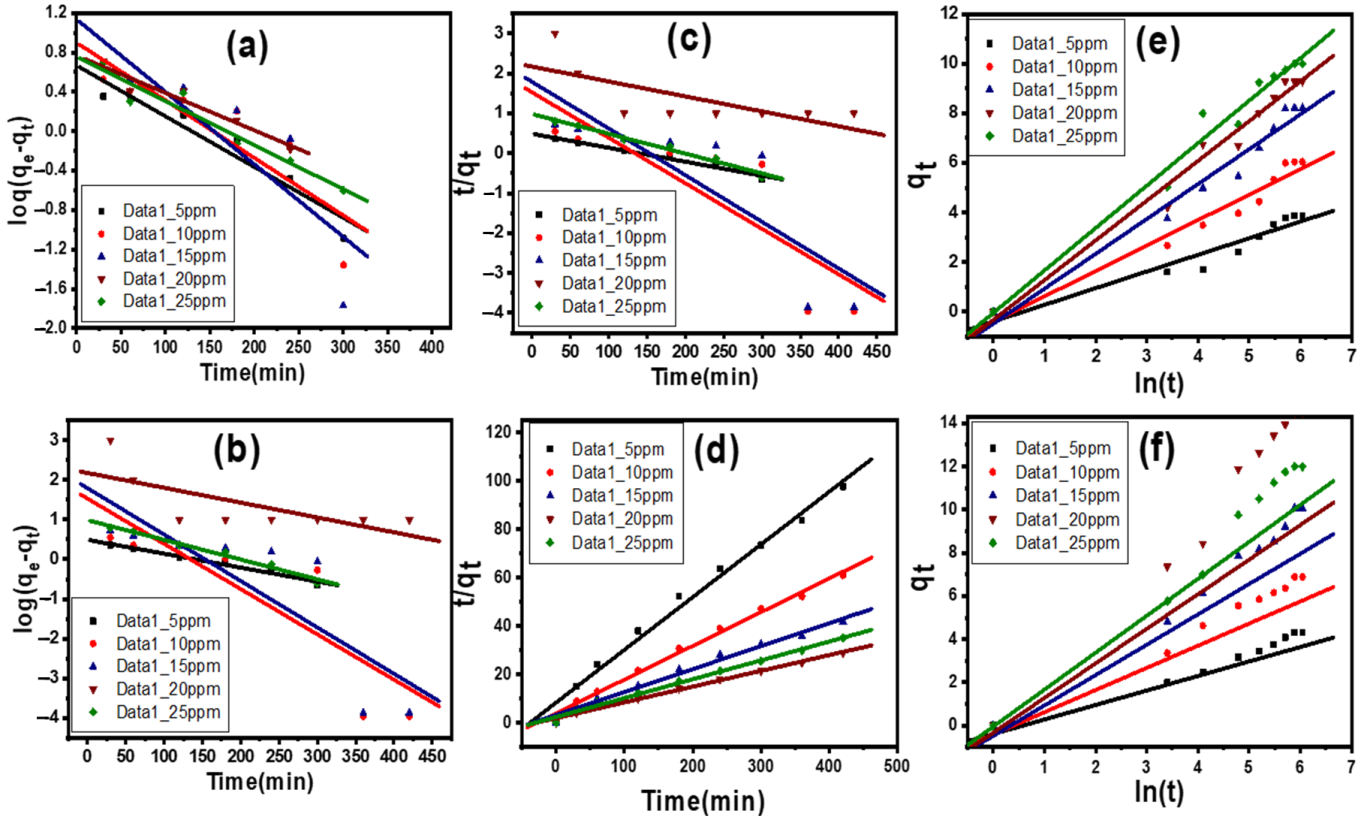

Figure 7. (**a**,**b**) Pseudo-first-order, (**c**,**d**) Pseudo-second-order, and (**e**,**f**) Elovich sorption kinetics of CR dye at 25 °C and pH 7 by 20 mg of (**a**,**c**,**e**) Gl and (**b**,**d**,**f**) Gl/PAN.

Table 3. Parameters of the kinetic models for CR dye adsorption on Gl and Gl/PAN.

Catalyst	Conc, ppm	First Order					Second Order					Elovich Kinetic Model			
		$q_e$exp	$q_{e\ calc.}$	k_1	R^2	Sd(yE±)	$q_e$exp	$q_{e\ calc.}$	k_2	R^2	Sd(yE±)	β (g/mg)	α (mg/min)	R^2	Sd(yE±)
Gl	25 ppm	10	2.84	0.0044	0.43	0.48473	10	10.47	0.0041	0.99	0.52443	0.5840	1.6662	0.97	3.2973
	20 ppm	9.28	3.53	0.0039	0.66	0.33911	9.28	9.90	0.0032	0.98	-	0.6236	1.3069	0.97	3.08573
	15 ppm	8.21	4.06	0.0066	0.28	0.90031	8.21	8.91	0.0027	0.97	1.96346	0.7107	1.0020	0.96	2.71908
	10 ppm	6.04	3.02	0.0052	0.29	0.69973	6.04	6.59	0.0032	0.97	1.8975	0.9741	0.6906	0.95	1.99781
	5 ppm	3.86	1.82	0.0038	0.24	0.56167	3.86	4.35	0.0039	0.96	0.37251	1.4881	0.3752	0.91	1.3324
Gl/PAN	25 ppm	12	4.95	0.0057	0.30	0.52443	12	12.81	0.0025	0.9915	11.7526	−1.829	−0.01189	0.98	4.01386
	20 ppm	11.57	2.71	0.0031	0.71	0.74402	11.57	15.33	0.002	0.99	9.81937	−1.9608	−0.00383	0.98	4.77362
	15 ppm	10.07	61.74	0.0269	0.70	1.96346	10.07	10.53	0.00278	0.98	14.3475	0.59573	1.3501	0.98	3.21219
	10 ppm	6.889	33.70	0.0262	0.71	1.8975	6.889	7.16	0.00497	0.99	21.01776	0.86258	1.0150	0.99	2.21156
	5 ppm	4.3	1.68	0.0028	0.30	0.37251	4.3	4.58	0.0056	0.98	32.96873	1.3752	0.5363	0.98	1.39569

The CR adsorption onto Gl and Gl/PAN adsorbents is well handled with the Pseudo-second-order diffusion model and this appears in the higher R^2 values from 5 ppm to 25 ppm concentration [85]. This was further reinforced by the good approximation between the estimated q_e and experimental q_{exp}.

3.5. Sorption Mechanism

To comprehend the rate-controlling steps and mechanisms that influence adsorption kinetics. Weber's Intra-particle diffusion was used to suit the experimental results. The availability to apply the Intra-particle diffusion concept is computed by a straight line in the plot of q_t vs. $t^{1/2}$ (Figure 8a,b). The slope and intercept of the plot can be used to calculate K_3 and I. The results are shown in Table 4. The intercept I value is not zero,

indicating that the intra-particle diffusion model may not be the primary rate-controlling mechanism in determining the adsorption process kinetics [86]. The boundary layer effect is reflected in the intercept in Figure 8. The bigger the contribution of surface adsorption in the rate control phase, the larger the intercept [86]. Figure 8 reveals a noticeable diffusion process following multi-linearity, which indicates that the adsorption process is controlled via more than one mass transfer step. At least two linear regions could be fitted with the experimental data [37]. From this can be inferred that the sorption process proceeds by film and intraparticle diffusion

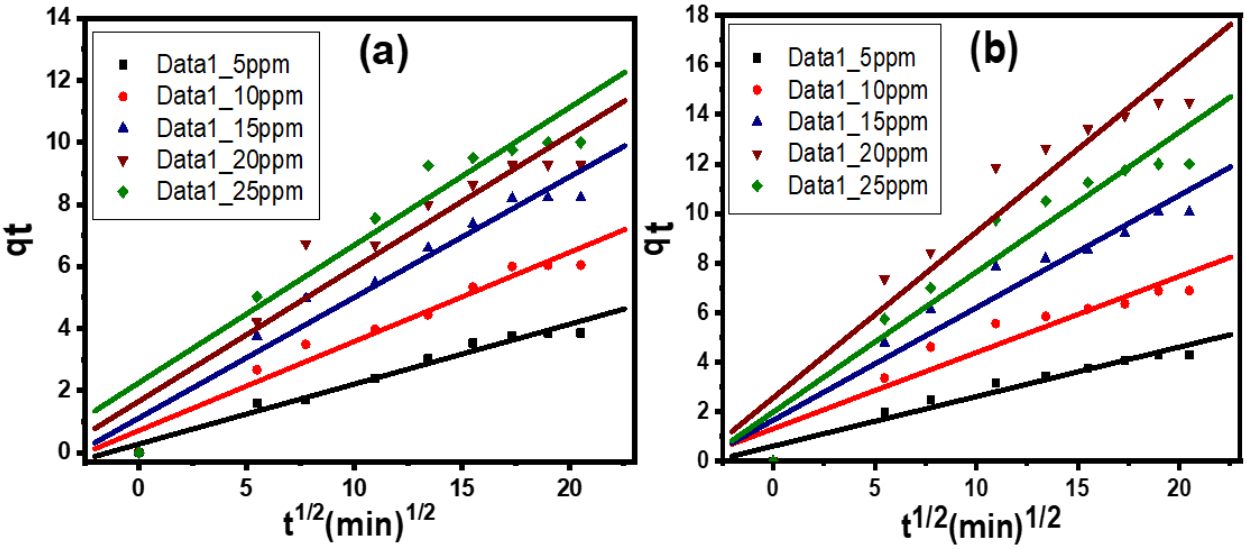

Figure 8. Intra-particle sorption kinetics of CR dye at 25 °C and pH 7 by 20 mg of (**a**) Gl and (**b**) Gl/PAN composite.

Table 4. Intra-particle diffusion constants for different initial CR concentrations at 25 °C.

Catalyst	Conc, ppm	Intraparticle Diffusion Kinetic Model		
		I	k_3 (mg/g $min^{1/2}$)	R^2
Gl	25	2.2523	0.4441	0.8361
	20	1.6566	0.4297	0.8936
	15	1.1161	0.3891	0.9440
	10	0.7108	0.2876	0.9550
	5	0.2779	0.1933	0.9707
Gl/PAN	25	1.9956	0.5646	0.9118
	20	2.5729	0.6684	0.9036
	15	1.667	0.4535	0.9188
	10	1.3227	0.3072	0.8895
	5	0.6206	0.1996	0.9427

3.6. Comparison of Adsorption Capability of Gl and Gl/PAN with Other Adsorbents

The Congo red dye adsorption capacity of different adsorbents was compared with Gl and Gl/PAN in Table 5. The Gl/PAN, arguably, has a higher adsorption capacity and a short contact time. As a result, Gl/PAN is a novel comforting adsorbent for CR dye removal from wastewater.

Table 5. Comparison of the optimized conditions, removal%, and adsorption capacity of different CR adsorbents relative to Gl and GL/PAN adsorbents.

Adsorbent	Conditions							Reference
	dye	C_o (mg/L)	dose (g/L)	pH	Time (min)	Q_m (mg/g)	R%	
Modified glauconite with thermal activation	RY160	10–80	1	1	180	-	64%	[66]
Modified glauconite with acetic acid activation	RY160	10–80	1	1	180	-	81%	[66]
Phosphate-modified kaolinite	CR	25–300	0.1	3–8	5–600	-	65%	[87]
Poly(N-isopropyl acrylamide-co-acrylic acid) microgel assemblies	Orange 2	-	-	-	-	-	73%	[88]
Poly(N-vinyl-2-pyrrolidone-co-acrylonitrile) treated with hydroxylamine–hydrochloride	Acid-fast Yellow G	-	-	-	-	7.6	-	[89]
PANI Nano fibers (PANI NFs)	CR	-	1	7	30	-	60%	[90]
Poly(N-vinyl-2-pyrrolidone-co-acrylonitrile) treated with hydroxylamine–hydrochloride	Direct Blue 3B	-	-	-	-	7	-	[91]
Poly(N-vinyl-2-pyrrolidone-co-acrylonitrile) treated with hydroxylamine–hydrochloride	Reactive red SH	-	-	-	-	7.4	-	[89]
Gl	CR	5–25	0.02	7	420	11.9	77%	Present study
Gl/PAN composite	CR	5–25	0.02	7	420	14.1	86%	

4. Conclusions

The hybrid Gl/PAN nanocomposite was prepared simply from environmentally friendly and low-cost raw materials. The morphological and structural features were studied by SEM, XRD, and FTIR. The values of average crystallite size were 15.6 nm and 12.6 nm for Gl and Gl/PAN. The performances of raw and modified glauconite in the adsorption of CR dye were investigated. The results show that initial dye concentration, contact time, adsorbent dosage, and pH all have a substantial impact on the adsorption process. The maximum uptake of the CR dye was observed at pH 8.0 for modified glauconite and pH 12 for raw glauconite. The removal efficiency of the dye reached the maximum with a Gl/PAN dose of 0.02 g. The experimental data were better fitted by the Langmuir model, which specified monolayer sorption. The maximum sorption capacity of CR dye was 11.9 and 14.1 mg/g for Gl and Gl/PAN, respectively. Furthermore, the adsorption kinetics could be well described for raw and modified glauconite by the pseudo-second-order kinetic. In addition to that, natural and modified glauconite can be regenerated for up to six cycles. According to the findings of this study, natural and modified glauconite with polyaniline can be used to successfully remove Congo red dye from textile effluent.

Author Contributions: Conceptualization, D.S., A.H., N.K.S., A.M.E., A.M.A., R.E.-S., S.A.A. and M.S.; methodology, D.S., A.H., N.K.S., A.M.A. and M.S.; validation, A.H., N.K.S. and M.S.; formal analysis, D.S., A.H., N.K.S., A.M.A. and M.S.; investigation, D.S., A.H., N.K.S., A.M.E., A.M.A., R.E.-S., S.A.A. and M.S.; resources, D.S., A.H., A.M.A., R.E.-S. and M.S.; data curation, D.S., A.H., N.K.S. and M.S.; writing—original draft preparation, D.S., A.H., N.K.S., A.M.A. and M.S.; writing—review and editing, D.S., A.H., N.K.S., A.M.E., A.M.A., R.E.-S., S.A.A. and M.S.; visualization, D.S., A.H., N.K.S. and M.S.; supervision, D.S., A.H., A.M.E., S.A.A. and M.S.; project administration, A.M.A. and M.S.; funding acquisition, A.M.A. and M.S. All authors have read and agreed to the published version of the manuscript.

Funding: The researchers wish to extend their sincere gratitude to the Deanship of Scientific Research at the Islamic University of Madinah for the support provided through the Research Groups Program: Grant no. (959/1443AH).

Data Availability Statement: The data presented in this study are available on request from the corresponding author.

Acknowledgments: This work is funded by the Deputyship of Research & Innovation, Ministry of Education in Saudi Arabia, through project number (959/1443). In addition, the authors would like to express their appreciation for the support provided by the Islamic University of Madinah.

Conflicts of Interest: The authors declare no conflict of interest.

Nomenclature

Gl	Glauconite
Gl/PAN	Glauconite/Polyaniline composite
CR	Congo Red dye
AN	Aniline
PPS	Potassium per sulfate
HCl	Hydrochloride acid
XRD	X-ray diffraction
SEM	Scanning electron microscopy
FT-IR	Fourier Transformer-Infrared Spectrometer
pHzpc	pH at zero point charge
ppm	Parts Per Million (1 milligram per liter)

References

1. Sonune, A.; Ghate, R. Developments in wastewater treatment methods. *Desalination* **2004**, *167*, 55–63. [CrossRef]
2. Crini, G. Recent developments in polysaccharide-based materials used as adsorbents in wastewater treatment. *Prog. Polym. Sci.* **2005**, *30*, 38–70. [CrossRef]
3. Campkin, B.; Cox, R. *Dirt: New Geographies of Cleanliness and Contamination*; IB Tauris: London, UK, 2007.
4. Rathoure, A.K.; Dhatwalia, V.K. *Toxicity and Waste Management Using Bioremediation*; Engineering Science Reference; IGI Global USA: Hershey, PA, USA, 2016.
5. Cox, M.; Négré, P.; Yurramendi, L. *Industrial Liquid Effluents*; INASMET Tecnalia: San Sebastian, Spain, 2007; p. 283.
6. Khalaf, M.N. *Green Polymers and Environmental Pollution Control*; CRC Press: Boca Raton, FL, USA, 2016.
7. Morin-Crini, N.; Crini, G.; Roy, L. Eaux industrielles contaminées. *PUFC Besançon* **2017**, *513*, 37–47.
8. Mustapha, S.; Ndamitso, M.; Abdulkareem, A.; Tijani, J.; Shuaib, D.; Ajala, A.; Mohammed, A. Application of TiO_2 and ZnO nanoparticles immobilized on clay in wastewater treatment: A review. *Appl. Water Sci.* **2020**, *10*, 49. [CrossRef]
9. Mukhopadhyay, R.; Bhaduri, D.; Sarkar, B.; Rusmin, R.; Hou, D.; Khanam, R.; Sarkar, S.; Biswas, J.K.; Vithanage, M.; Bhatnagar, A. Clay–polymer nanocomposites: Progress and challenges for use in sustainable water treatment. *J. Hazard. Mater.* **2020**, *383*, 121125. [CrossRef]
10. Sokolowska-Gajda, J.; Freeman, H.S.; Reife, A. Synthetic dyes based on environmental considerations. Part 2: Iron complexes formazan dyes. *Dyes Pigment.* **1996**, *30*, 1–20. [CrossRef]
11. Ivanov, K.; Gruber, E.; Schempp, W.; Kirov, D. Possibilities of using zeolite as filler and carrier for dyestuffs in paper. *Papier* **1996**, *50*, 56–60.
12. Kabdaşli, I.; Tünay, O.; Orhon, D. Wastewater control and management in a leather tanning district. *Water Sci. Technol.* **1999**, *40*, 261–267. [CrossRef]
13. Bensalah, N.; Alfaro, M.Q.; Martínez-Huitle, C. Electrochemical treatment of synthetic wastewaters containing Alphazurine A dye. *Chem. Eng. J.* **2009**, *149*, 348–352. [CrossRef]

14. Wróbel, D.; Boguta, A.; Ion, R.M. Mixtures of synthetic organic dyes in a photoelectrochemical cell. *J. Photochem. Photobiol. A Chem.* **2001**, *138*, 7–22. [CrossRef]
15. Dawood, S.; Sen, T.K.; Phan, C. Synthesis and characterisation of novel-activated carbon from waste biomass pine cone and its application in the removal of congo red dye from aqueous solution by adsorption. *Water Air Soil Pollut.* **2014**, *225*, 1818. [CrossRef]
16. Benefield, L.D.; Judkins, J.F.; Weand, B.L. *Process Chemistry for Water and Wastewater Treatment*; Prentice Hall: Hoboken, NJ, USA, 1982.
17. Liu, D.H.; Lipták, B.G. *Hazardous Waste and Solid*; CRC Press: Boca Raton, FL, USA, 1999.
18. Henze, M.; Harremoes, P.; la Cour Jansen, J.; Arvin, E. *Wastewater Treatment: Biological and Chemical Processes*, 3rd ed.; Springer: Berlin/Heidelberg, Germany, 2001.
19. Harvey, P.J.; Campanella, B.F.; Castro, P.M.; Harms, H.; Lichtfouse, E.; Schäffner, A.R.; Smrcek, S.; Werck-Reichhart, D. Phytoremediation of polyaromatic hydrocarbons, anilines and phenols. *Environ. Sci. Pollut. Res.* **2002**, *9*, 29–47. [CrossRef] [PubMed]
20. Hamd, A.; Shaban, M.; AlMohamadi, H.; Dryaz, A.R.; Ahmed, S.A.; Al-Ola, K.A.A.; El-Mageed, H.R.A.; Soliman, N.K. Novel Wastewater Treatment by Using Newly Prepared Green Seaweed–Zeolite Nanocomposite. *ACS Omega* **2022**, *7*, 11044–11056. [CrossRef] [PubMed]
21. Anjaneyulu, Y.; Sreedhara Chary, N.; Samuel Suman Raj, D. Decolourization of industrial effluents–available methods and emerging technologies—A review. *Rev. Environ. Sci. Bio Technol.* **2005**, *4*, 245–273. [CrossRef]
22. Hai, F.I.; Yamamoto, K.; Fukushi, K. Hybrid treatment systems for dye wastewater. *Crit. Rev. Environ. Sci. Technol.* **2007**, *37*, 315–377. [CrossRef]
23. Barakat, M. New trends in removing heavy metals from industrial wastewater. *Arab. J. Chem.* **2011**, *4*, 361–377. [CrossRef]
24. Salleh, M.A.M.; Mahmoud, D.K.; Karim, W.A.W.A.; Idris, A. Cationic and anionic dye adsorption by agricultural solid wastes: A comprehensive review. *Desalination* **2011**, *280*, 1–13. [CrossRef]
25. Feng, Y.; Zhou, H.; Liu, G.; Qiao, J.; Wang, J.; Lu, H.; Yang, L.; Wu, Y. Methylene blue adsorption onto swede rape straw (Brassica napus L.) modified by tartaric acid: Equilibrium, kinetic and adsorption mechanisms. *Bioresour. Technol.* **2012**, *125*, 138–144. [CrossRef]
26. Ghosh, R.K.; Reddy, D.D. Crop Residue Ashes as Adsorbents for Basic Dye (M ethylene Blue) Removal: Adsorption Kinetics and Dynamics. *CLEAN—Soil Air Water* **2014**, *42*, 1098–1105. [CrossRef]
27. Ali, I.; Asim, M.; Khan, T.A. Low cost adsorbents for the removal of organic pollutants from wastewater. *J. Environ. Manag.* **2012**, *113*, 170–183. [CrossRef]
28. Tehrani-Bagha, A.; Nikkar, H.; Mahmoodi, N.; Markazi, M.; Menger, F. The sorption of cationic dyes onto kaolin: Kinetic, isotherm and thermodynamic studies. *Desalination* **2011**, *266*, 274–280. [CrossRef]
29. Gupta, V. Application of low-cost adsorbents for dye removal–a review. *J. Environ. Manag.* **2009**, *90*, 2313–2342. [CrossRef] [PubMed]
30. Parab, H.; Sudersanan, M.; Shenoy, N.; Pathare, T.; Vaze, B. Use of agro-industrial wastes for removal of basic dyes from aqueous solutions. *CLEAN—Soil Air Water* **2009**, *37*, 963–969. [CrossRef]
31. Rafatullah, M.; Sulaiman, O.; Hashim, R.; Ahmad, A. Adsorption of methylene blue on low-cost adsorbents: A review. *J. Hazard. Mater.* **2010**, *177*, 70–80. [CrossRef] [PubMed]
32. Verma, M.; Tyagi, I.; Chandra, R.; Gupta, V.K. Adsorptive removal of Pb (II) ions from aqueous solution using CuO nanoparticles synthesized by sputtering method. *J. Mol. Liq.* **2017**, *225*, 936–944. [CrossRef]
33. Van der Merwe, D.; Pickrell, J.A. Toxicity of Nanomaterials. In *Veterinary Toxicology*, 3rd ed.; Gupta, R.C., Ed.; Academic Press: Cambridge, MA, USA, 2018; pp. 319–326.
34. Roy, R.; Roy, R.A.; Roy, D.M. Alternative perspectives on "quasi-crystallinity": Non-uniformity and nanocomposites. *Mater. Lett.* **1986**, *4*, 323–328. [CrossRef]
35. Hajjaoui, H.; Soufi, A.; Boumya, W.; Abdennouri, M.; Barka, N. Polyaniline/Nanomaterial Composites for the Removal of Heavy Metals by Adsorption: A Review. *J. Compos. Sci.* **2021**, *5*, 233. [CrossRef]
36. Xu, H.; Zhu, S.; Lu, K.; Jia, H.; Xia, M.; Wang, F. Preparation of hierarchically floral ZIF-8 derived carbon@polyaniline@Ni/Al layered double hydroxides composite with outstanding removal phenomenon for saccharin. *Chem. Eng. J.* **2022**, *450*, 138127. [CrossRef]
37. Xu, H.; Zhu, S.; Xia, M.; Wang, F.; Ju, X. Three-dimension hierarchical composite via in-situ growth of Zn/Al layered double hydroxide plates onto polyaniline-wrapped carbon sphere for efficient naproxen removal. *J. Hazard. Mater.* **2022**, *423*, 127192. [CrossRef]
38. Zehhaf, A.; Benyoucef, A.; Quijada, C.; Taleb, S.; Morallon, E. Algerian natural montmorillonites for arsenic (III) removal in aqueous solution. *Int. J. Environ. Sci. Technol.* **2015**, *12*, 595–602. [CrossRef]
39. Franus, M.; Bandura, L.; Madej, J. Mono and poly-cationic adsorption of heavy metals using natural glauconite. *Minerals* **2019**, *9*, 470. [CrossRef]
40. Selby, D. U-Pb zircon geochronology of the Aptian/Albian boundary implies that the GL-O international glauconite standard is anomalously young. *Cretac. Res.* **2009**, *30*, 1263–1267. [CrossRef]

41. Sobeih, M.M.; El-Shahat, M.; Osman, A.; Zaid, M.; Nassar, M.Y. Glauconite clay-functionalized chitosan nanocomposites for efficient adsorptive removal of fluoride ions from polluted aqueous solutions. *RSC Adv.* **2020**, *10*, 25567–25585. [CrossRef] [PubMed]
42. Stejskal, J.; Polyaniline, G.R.G. Preparation of a conducting polymer (IUPAC technical report). *Pure Appl. Chem.* **2002**, *74*, 857–867. [CrossRef]
43. Bhadra, S.; Singha, N.K.; Khastgir, D. Electrochemical synthesis of polyaniline and its comparison with chemically synthesized polyaniline. *J. Appl. Polym. Sci.* **2007**, *104*, 1900–1904. [CrossRef]
44. Khedr, M.; Halim, K.A.; Soliman, N. Synthesis and photocatalytic activity of nano-sized iron oxides. *Mater. Lett.* **2009**, *63*, 598–601. [CrossRef]
45. Soliman, N.k.; Moustafa, A.F.; Aboud, A.A.; Halim, K.S.A. Effective utilization of Moringa seeds waste as a new green environmental adsorbent for removal of industrial toxic dyes. *J. Mater. Res. Technol.* **2019**, *8*, 1798–1808. [CrossRef]
46. Kausar, A.; Sher, F.; Hazafa, A.; Javed, A.; Sillanpää, M.; Iqbal, M. Biocomposite of sodium-alginate with acidified clay for wastewater treatment: Kinetic, equilibrium and thermodynamic studies. *Int. J. Biol. Macromol.* **2020**, *161*, 1272–1285. [CrossRef]
47. Wang, S.G.; Liu, X.W.; Gong, W.X.; Nie, W.; Gao, B.Y.; Yue, Q.Y. Adsorption of fulvic acids from aqueous solutions by carbon nanotubes, Journal of Chemical Technology & Biotechnology: International Research in Process. *Environ. Clean Technol.* **2007**, *82*, 698–704.
48. Freundlich, H. Over the adsorption in solution. *J. Phys. Chem.* **1906**, *57*, 1100–1107.
49. Li, Z.; Chang, P.-H.; Jiang, W.-T.; Jean, J.-S.; Hong, H. Mechanism of methylene blue removal from water by swelling clays. *Chem. Eng. J.* **2011**, *168*, 1193–1200. [CrossRef]
50. Langmuir, I. The adsorption of gases on plane surfaces of glass, mica and platinum. *J. Am. Chem. Soc.* **1918**, *40*, 1361–1403. [CrossRef]
51. Temkin, M. Kinetics of ammonia synthesis on promoted iron catalysts. *Acta Physiochim. URSS* **1940**, *12*, 327–356.
52. Foo, K.; Hameed, B. Preparation, characterization and evaluation of adsorptive properties of orange peel based activated carbon via microwave induced K2CO3 activation. *Bioresour. Technol.* **2012**, *104*, 679–686. [CrossRef] [PubMed]
53. Singh, S.A.; Vemparala, B.; Madras, G. Adsorption kinetics of dyes and their mixtures with Co_3O_4–ZrO_2 composites. *J. Environ. Chem. Eng.* **2015**, *3*, 2684–2696. [CrossRef]
54. Ozdemir, O.; Armagan, B.; Turan, M.; Celik, M.S. Comparison of the adsorption characteristics of azo-reactive dyes on mezoporous minerals. *Dyes Pigment.* **2004**, *62*, 49–60. [CrossRef]
55. Ho, Y.; McKay, G. Comparative sorption kinetic studies of dye and aromatic compounds onto fly ash. *J. Environ. Sci. Health Part A* **1999**, *34*, 1179–1204. [CrossRef]
56. Ho, Y.-S.; McKay, G. Pseudo-second order model for sorption processes. *Process Biochem.* **1999**, *34*, 451–465. [CrossRef]
57. Ismadji, S.; Bhatia, S. A modified pore-filling isotherm for liquid-phase adsorption in activated carbon. *Langmuir* **2001**, *17*, 1488–1498. [CrossRef]
58. Yuh-Shan, H. Citation review of lagergren kinetic rate equation on adsorption reactions. *Scientometrics* **2004**, *59*, 171–177. [CrossRef]
59. Essandoh, M.; Kunwar, B.; Pittman, C.U., Jr.; Mohan, D.; Mlsna, T. Sorptive removal of salicylic acid and ibuprofen from aqueous solutions using pine wood fast pyrolysis biochar. *Chem. Eng. J.* **2015**, *265*, 219–227. [CrossRef]
60. Gan, C.; Liu, Y.; Tan, X.; Wang, S.; Zeng, G.; Zheng, B.; Li, T.; Jiang, Z.; Liu, W. Effect of porous zinc–biochar nanocomposites on Cr (VI) adsorption from aqueous solution. *RSC Adv.* **2015**, *5*, 35107–35115. [CrossRef]
61. Belousov, P.; Semenkova, A.; Egorova, T.; Romanchuk, A.; Zakusin, S.; Dorzhieva, O.; Tyupina, E.; Izosimova, Y.; Tolpeshta, I.; Chernov, M. Cesium sorption and desorption on glauconite, bentonite, zeolite, and diatomite. *Minerals* **2019**, *9*, 625. [CrossRef]
62. Mostafaei, A.; Zolriasatein, A. Synthesis and characterization of conducting polyaniline nanocomposites containing ZnO nanorods. *Prog. Nat. Sci. Mater. Int.* **2012**, *22*, 273–280. [CrossRef]
63. Younes, H.; El-Etriby, H.K.; Mahanna, H. High removal efficiency of reactive yellow 160 dye from textile wastewater using natural and modified glauconite. *Int. J. Environ. Sci. Technol.* **2022**, *19*, 5659–5674. [CrossRef]
64. Younes, H.; Mahanna, H.; El-Etriby, H.K. Fast adsorption of phosphate (PO4−) from wastewater using glauconite. *Water Sci. Technol.* **2019**, *80*, 1643–1653. [CrossRef]
65. Shekhar, S.; Mishra, D.; Agrawal, A.; Sahu, K. Physical and chemical characterization and recovery of potash fertilizer from glauconitic clay for agricultural application. *Appl. Clay Sci.* **2017**, *143*, 50–56. [CrossRef]
66. Selim, K.; Youssef, M.; El-Rahiem, F.A.; Hassan, M. Dye removal using some surface modified silicate minerals. *Int. J. Min. Sci. Technol.* **2014**, *24*, 183–189. [CrossRef]
67. Borth, K.W.; Galdino, C.W.; de Carvalho Teixeira, V.; Anaissi, F.J. Iron oxide nanoparticles obtained from steel waste recycling as a green alternative for Congo red dye fast adsorption. *Appl. Surf. Sci.* **2021**, *546*, 149126. [CrossRef]
68. Sharma, Y.C. Optimization of parameters for adsorption of methylene blue on a low-cost activated carbon. *J. Chem. Eng. Data* **2010**, *55*, 435–439. [CrossRef]
69. Vikas, B.; Fasullo, M. (Eds.) *Cell Growth*; IntechOpen: London, UK, 2020.
70. Pons, M.P.; Fuste, M.C. Uranium uptake by immobilized cells of Pseudomonas strain EPS 5028. *Appl. Microbiol. Biotechnol.* **1993**, *39*, 661–665. [CrossRef]

71. Tahir, M.A.; Bhatti, H.N.; Iqbal, M. Solar Red and Brittle Blue direct dyes adsorption onto Eucalyptus angophoroides bark: Equilibrium, kinetics and thermodynamic studies. *J. Environ. Chem. Eng.* **2016**, *4*, 2431–2439. [CrossRef]
72. Mohamed, H.S.; Soliman, N.; Abdelrheem, D.A.; Ramadan, A.A.; Elghandour, A.H.; Ahmed, S.A. Adsorption of Cd^{2+} and Cr^{3+} ions from aqueous solutions by using residue of Padina gymnospora waste as promising low-cost adsorbent. *Heliyon* **2019**, *5*, e01287. [CrossRef] [PubMed]
73. Gong, R.; Ding, Y.; Liu, H.; Chen, Q.; Liu, Z. Lead biosorption and desorption by intact and pretreated Spirulina maxima biomass. *Chemosphere* **2005**, *58*, 125–130. [CrossRef]
74. Meikle, A.J.; Gadd, G.M.; Reed, R.H. Manipulation of yeast for transport studies: Critical assessment of cultural and experimental procedures. *Enzym. Microb. Technol.* **1990**, *12*, 865–872. [CrossRef]
75. Fourest, E.; Roux, J.-C. Heavy metal biosorption by fungal mycelial by-products: Mechanisms and influence of pH. *Appl. Microbiol. Biotechnol.* **1992**, *37*, 399–403. [CrossRef]
76. Nandi, B.; Goswami, A.; Purkait, M. Removal of cationic dyes from aqueous solutions by kaolin: Kinetic and equilibrium studies. *Appl. Clay Sci.* **2009**, *42*, 583–590. [CrossRef]
77. Karthikaikumar, S.; Karthikeyan, M.; Kumar, K.S. Removal of congo red dye from aqueous solution by polyaniline–montmorrillonite composite. *Chem. Sci. Rev. Lett.* **2014**, *2*, 606–614.
78. Kalotra, S.; Mehta, R. Synthesis of polyaniline/clay nanocomposites by in situ polymerization and its application for the removal of Acid Green 25 dye from wastewater. *Polym. Bull.* **2021**, *78*, 2439–2463. [CrossRef]
79. Foo, K.Y.; Hameed, B.H. Insights into the modeling of adsorption isotherm systems. *Chem. Eng. J.* **2010**, *156*, 2–10. [CrossRef]
80. Sprynskyy, M.; Buszewski, B.; Terzyk, A.P.; Namieśnik, J. Study of the selection mechanism of heavy metal (Pb^{2+}, Cu^{2+}, Ni^{2+}, and Cd^{2+}) adsorption on clinoptilolite. *J. Colloid Interface Sci.* **2006**, *304*, 21–28. [CrossRef] [PubMed]
81. Zhang, J.; Zhou, Q.; Ou, L. Kinetic, isotherm, and thermodynamic studies of the adsorption of methyl orange from aqueous solution by chitosan/alumina composite. *J. Chem. Eng. Data* **2012**, *57*, 412–419. [CrossRef]
82. Alkan, M.; Demirbaş, Ö.; Çelikçapa, S.; Doğan, M. Sorption of acid red 57 from aqueous solution onto sepiolite. *J. Hazard. Mater.* **2004**, *116*, 135–145. [CrossRef] [PubMed]
83. Shirsath, S.; Patil, A.; Bhanvase, B.; Sonawane, S. Ultrasonically prepared poly (acrylamide)-kaolin composite hydrogel for removal of crystal violet dye from wastewater. *J. Environ. Chem. Eng.* **2015**, *3*, 1152–1162. [CrossRef]
84. Naghizadeh, A. Regeneration of carbon nanotubes exhausted with humic acid using electro-Fenton technology. *Arab. J. Sci. Eng.* **2016**, *41*, 155–161. [CrossRef]
85. Raval, N.P.; Kumar, M. Geogenic arsenic removal through core–shell based functionalized nanoparticles: Groundwater in-situ treatment perspective in the post–COVID Anthropocene. *J. Hazard. Mater.* **2021**, *402*, 123466. [CrossRef]
86. Weber, W.J., Jr.; Morris, J.C. Kinetics of adsorption on carbon from solution. *J. Sanit. Eng. Div.* **1963**, *89*, 31–59. [CrossRef]
87. Shaban, M.; Sayed, M.I.; Shahien, M.G.; Abukhadra, M.R.; Ahmed, Z.M. Adsorption behavior of inorganic-and organic-modified kaolinite for Congo red dye from water, kinetic modeling, and equilibrium studies. *J. Sol-Gel Sci. Technol.* **2018**, *87*, 427–441. [CrossRef]
88. Parasuraman, D.; Sarker, A.K.; Serpe, M.J. Poly (N-Isopropylacrylamide)-Based Microgels and Their Assemblies for Organic-Molecule Removal from Water. *ChemPhysChem* **2012**, *13*, 2507–2515. [CrossRef]
89. El-Aal, S.E.A.; Hegazy, E.S.A.; AbuTaleb, M.; Dessouki, A. Radiation synthesis of copolymers for adsorption of dyes from their industrial wastes. *J. Appl. Polym. Sci.* **2005**, *96*, 753–763. [CrossRef]
90. Bhaumik, M.; McCrindle, R.I.; Maity, A. Enhanced adsorptive degradation of Congo red in aqueous solutions using polyaniline/Fe0 composite nanofibers. *Chem. Eng. J.* **2015**, *260*, 716–729. [CrossRef]
91. Valderrama, C.; Cortina, J.; Farran, A.; Gamisans, X.; de Las Heras, F. Kinetic study of acid red "dye" removal by activated carbon and hyper-cross-linked polymeric sorbents Macronet Hypersol MN200 and MN300. *React. Funct. Polym.* **2008**, *68*, 718–731. [CrossRef]